iScience

CellPress
OPEN ACCESS

Article

Intracellular metabolic adaptation of intraepithelial CD4$^+$CD8$\alpha\alpha^+$ T lymphocytes

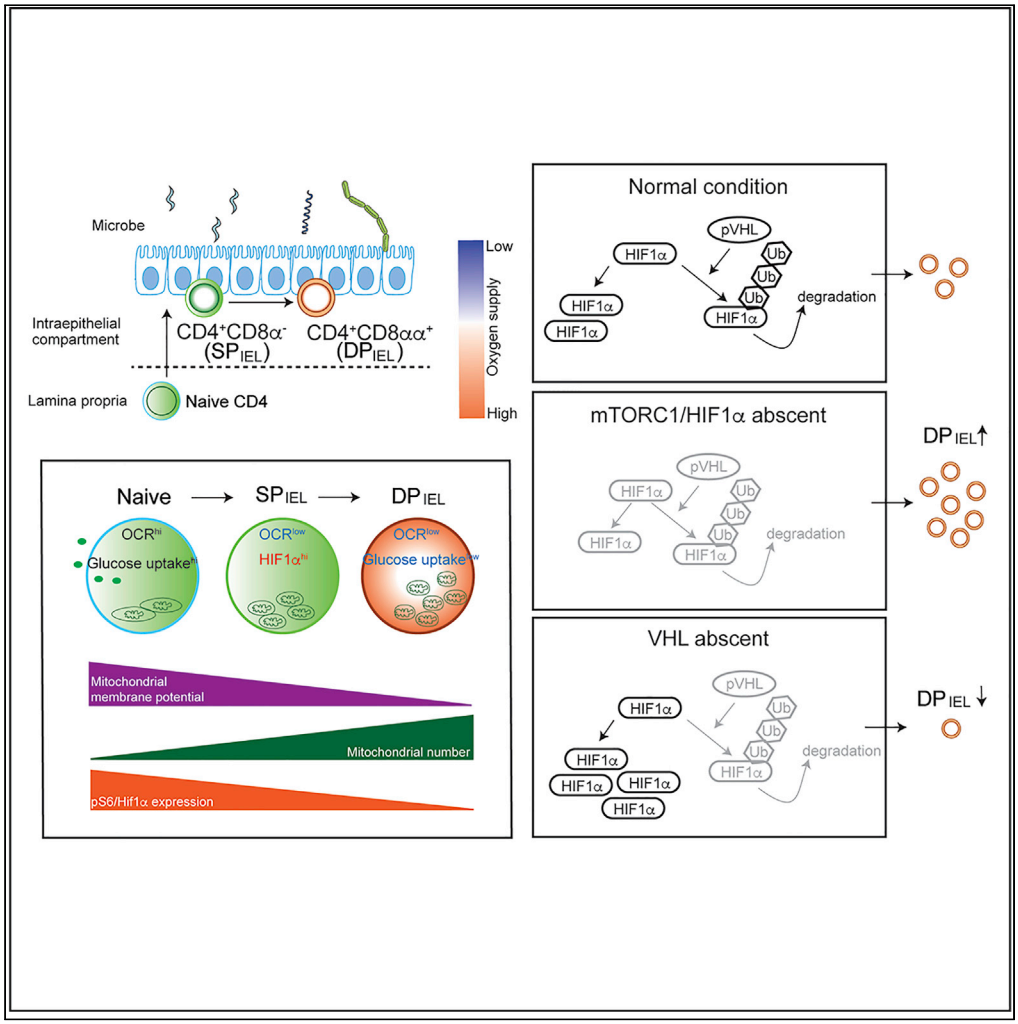

Yosuke Harada, Tomohisa Sujino, Kentaro Miyamoto, ..., Atsushi Hirao, Yoshiaki Kubota, Takanori Kanai

tsujino1224@keio.jp (T.S.)
takagast@keio.jp (T.K.)

Highlights

Microbes induce hypoxic conditions in the intraepithelial compartment

Induced IELs show a lower OCR, glucose uptake, and mitochondrial membrane potential

DP$_{IELs}$ show reduced expression of *Hif1α/Hif2α* during development

Downregulation of *Rptor* and *Hif1α/Hif2α* expression in CD4$^+$ T cells induces DP$_{IELs}$

Harada et al., iScience *25*, 104021
April 15, 2022
https://doi.org/10.1016/j.isci.2022.104021

iScience

CellPress
OPEN ACCESS

Article

Intracellular metabolic adaptation of intraepithelial CD4$^+$CD8αα$^+$ T lymphocytes

Yosuke Harada,[1,7] Tomohisa Sujino,[2,8,*] Kentaro Miyamoto,[1,3,7] Ena Nomura,[1,7] Yusuke Yoshimatsu,[1] Shun Tanemoto,[1] Satoko Umeda,[1] Keiko Ono,[1] Yohei Mikami,[1] Nobuhiro Nakamoto,[1] Kaoru Takabayashi,[2] Naoki Hosoe,[2] Haruhiko Ogata,[2] Tuneo Ikenoue,[4] Atsushi Hirao,[5] Yoshiaki Kubota,[6] and Takanori Kanai[1,*]

SUMMARY

Intestinal intraepithelial lymphocytes (IELs), the first line of defense against microbial and dietary antigens, are classified as natural or induced based on their origin and receptor expression. Induced CD4$^+$CD8αα$^+$TCRβ$^+$ T cells (double positive, DP$_{IELs}$) originated from CD4$^+$CD8α$^-$TCRβ$^+$ T cells (single positive, SP$_{IELs}$) increase with aging. However, the metabolic requirements and the metabolic-related genes in IEL development remain unclear. We determined that the intraepithelial compartment is hypoxic in the presence of microbes and DP$_{IELs}$ increased more than natural IELs in this location. Moreover, DP$_{IELs}$ consumed less oxygen and glucose and exhibited unique alterations in mitochondria. Using inhibitors and genetically modified mice, we revealed that DP$_{IELs}$ adapt to their surrounding oxygen-deprived environment in peripheral tissues by modulating specific genes, including hypoxia-inducible factor, mammalian target of rapamycin complexes (mTORC), phosphorylated ribosomal protein S6 (pS6), and other glycolytic factors. Our findings provide valuable insight into the metabolic properties of IELs.

INTRODUCTION

The intestinal mucosal barrier, which has a poor blood supply, is formed by a dense mucus layer, organized epithelial cells, and intraepithelial lymphocytes (IELs) (Cheroutre et al., 2011). IELs are located in the intraepithelial compartment and are the first line of defense against bacterial or food antigens. IELs are classified as natural IELs and induced IELs. Natural IELs, including TCRγδ$^+$ cells and CD8αα$^+$ T cells, develop in the thymus, and induced IELs, such as CD8αβ$^+$TCRβ$^+$ cells and CD4$^+$CD8αα$^+$TCRβ$^+$ T cells (double positive cells, DP$_{IELs}$), develop in the periphery (Olivares-Villagomez and Van Kaer, 2018; Van Kaer and Olivares-Villagomez, 2018). DP$_{IELs}$ originate from CD4$^+$CD8α$^-$TCRβ$^+$ T cells (single positive IELs, SP$_{IELs}$) and accumulate with aging (Konkel et al., 2011). DP$_{IELs}$ express both CD4 and CD8αα via the downregulation of T helper POZ/Kruppel like factor (*Thpok* also known as *Zbtb7b*) and upregulation of Runt-related transcription factor (*Runx3*) during their development (Bilate et al., 2016; Cervantes-Barragan et al., 2017; Sujino et al., 2016). IELs express activation markers such as CD44 and CD69 (Cheroutre et al., 2011), also they express enzymes and cytokines, such as granzyme B and interleukin (IL)-17A, depending on the cell type. They proliferate less compared with other T cells, and originate from long-lived tissue-resident effector memory cells (Groux et al., 1997; Konjar et al., 2018; Mucida et al., 2013; Reis et al., 2013; Sydora et al., 1993; Vandereyken et al., 2020; Yu et al., 2008).

Metabolic reprogramming is essential for T cell activation and function. The activation of naïve CD4$^+$ T cells in lymphoid tissues leads to metabolic reprogramming from oxidative phosphorylation (OXPHOS) to anabolic metabolism. For instance, Foxp3-positive regulatory T cells (Tregs) preferentially use OXPHOS, and effector T cell subsets [T helper type (Th) 1), Th2, Th17, and CD8$^+$ T cells] preferentially undergo glycolysis with lactate production (Jung et al., 2019; MacIver et al., 2013; Pearce and Pearce, 2013; Shi et al., 2011). The metabolic requirements of T cell subsets were previously studied using *in vitro* cultured cells or cells isolated from spleen and lymphoid tissues. In addition, cells alter their energy usage in response to environmental factors. Tregs mainly use OXPHOS in oxygen-rich conditions, whereas in glucose-deprived and oxygen-deprived environments, such as cancer or peripheral tissues, Tregs rely on lactate as an alternate energy source (Angelin et al., 2017; Newton et al., 2016). Hypoxia inducible factor 1 subunit alpha (*Hif1α*) is

[1]Department of Gastroenterology, Keio University School of Medicine, 35, Shinanomachi, Shinjuku-ku, Tokyo 160-8582, Japan

[2]Center for Diagnostic and Therapeutic Endoscopy, Keio University Hospital, 35, Shinanomachi, Shinjuku-ku, Tokyo 160-8582, Japan

[3]Miyarisan Pharmaceutical Co. Ltd. Tokyo 114-0016, Japan

[4]Division of Clinical Genome Research, The Institute of Medical Science, The University of Tokyo, Tokyo, Japan

[5]Division of Molecular Genetics, Cancer Research Institute, Kanazawa University, Kanazawa, Japan

[6]Department of Anatomy, Keio University School of Medicine, Tokyo 160-8582, Japan

[7]These authors contributed equally

[8]Lead contact

*Correspondence: tsujino1224@keio.jp (T.S.), takagast@keio.jp (T.K.)

https://doi.org/10.1016/j.isci.2022.104021

a key gene in the regulation of glycolysis and mitochondrial respiration in hypoxic tissue environments. Under hypoxic conditions, Tregs switch their metabolic status to glycolysis and upregulate *Hif1α*. This metabolic shift is essential for Tregs to migrate and survive in hypoxic tissues (Dodd et al., 2015; He et al., 2018). The oxygen and glucose consumption levels of natural and peripheral IELs and how metabolic-related genes affect the development of induced IELs remain unclear.

Here, we first show that the intraepithelial compartment is hypoxic in the presence of microbes. Induced IELs, DP_{IELs}, and SP_{IELs} showed a reduced oxygen consumption rate (OCR), glucose uptake, and extracellular acidification rate (ECAR). DP_{IELs} exhibited an increased number of mitochondria compared with naive $CD4^+$ T cells, and SP_{IELs} and DP_{IELs} showed enhanced expression of fission related-genes and a low mitochondrial membrane potential compared with naive $CD4^+$ T cells. Although DP_{IELs} showed reduced glucose uptake compared with naive $CD4^+$ T cells, 2-deoxy-D-glucose (2DG), which blocks glucose uptake, inhibited the development of DP_{IELs}. Under hypoxic conditions, cells expressed *Hif1α/Hif2α* to adapt to the tissue environment. Interestingly, DP_{IELs} showed reduced expression levels of *Hif1α/Hif2α* and phosphorylated ribosomal protein S6 (pS6) during development. Genetic ablation of *Rptor* or *Hif1α/Hif2α* in $CD4^+$ T cells increased the percentage of DP_{IELs}. We uncovered that DP_{IELs} develop as a unique population and adapt to low oxygen circumstances by decreasing oxygen and glucose consumption, but the expression levels of *Hif1α/Hif2α* and phosphorylation level of S6 are reduced during their development from SP_{IELs}. Our findings indicate that peripheral tissue-resident cells develop by adapting to the environmental niche, such as hypoxic conditions, with alterations in metabolic-related gene expression.

RESULTS

Intestinal intraepithelial compartment is hypoxic in SPF mice

We first analyzed the intestinal oxygen supply in the presence of microbes. Although the oxygen concentration of the lamina propria compartment was equivalent in specific-pathogen-free (SPF) mice and germ-free (GF) mice, the oxygen concentration of the intraepithelial compartment was decreased in SPF mice compared with GF mice (Figures 1A and 1B). These data indicate that the intraepithelial compartment is deprived of oxygen in the presence of microbes. Intraepithelial cells develop and reside in a suitable location with low oxygenic conditions in SPF mice. Therefore, we questioned which cell types develop in the low oxygenic intraepithelial compartment in SPF mice. The numbers of cells in the intraepithelial compartment in GF mice and SPF mice were analyzed (Figure 1C). We divided the cell number in SPF mice and GF mice in each population. The numbers of natural IELs, including $TCR\gamma\delta^+$ T cells and $CD8\alpha\alpha^+$ $TCR\beta^+$ T cells, were increased by 3-fold to 5-fold in SPF mice compared with GF mice (Figure 1D). Furthermore, induced IELs, such as $CD4^+TCR\beta^+$ T cells and $CD8\alpha\beta^+TCR\beta^+$ T cells, were increased by 15-fold to 20-fold in SPF mice compared with GF mice (Figure 1D). $CD4^+TCR\beta^+$ IELs are divided into two populations: terminally differentiated IELs that express $CD4^+CD8\alpha\alpha^+TCR\beta^+$ (DP_{IELs}) and $CD4^+CD8\alpha\alpha^-TCR\beta^+$ cells (SP_{IELs}). Significantly, DP_{IELs} were increased by more than a thousand times in SPF mice compared with GF mice. These data indicate induced IELs, especially DP_{IELs}, develop in low oxygenic conditions.

$CD4^+CD8\alpha\alpha^+TCR\beta^+$ IELs exhibit a reduced OCR and ECAR

We then determined the OCR of IELs in the intraepithelial compartment because $CD4^+TCR\beta^+$ T cells, especially DP_{IELs}, develop in low oxygen conditions. We measured the OCR in splenic naive $CD4^+$ T cells, $TCR\gamma\delta^+$ T cells, $CD8\alpha\beta^+$ T cells, SP_{IELs}, and DP_{IELs} from small intestine epithelium. SP_{IELs} and DP_{IELs} showed a reduced OCR compared with naive $CD4^+$ T cells and $TCR\gamma\delta^+$ T cells. DP_{IELs} displayed a slightly lower OCR compared with SP_{IELs}, but the result was not significant (Figure 2A). $CD8\alpha\beta^+$ T cells tended to show a higher OCR than SP_{IELs} and DP_{IELs}. We next measured glycolysis by determining the ECAR and glucose intake using 2-NBDG in each cell type. SP_{IELs} and DP_{IELs} showed a lower ECAR than naïve $CD4^+$ T cells and $TCR\gamma\delta^+$ T cells (Figure 2B). The ECAR in $CD8\alpha\beta^+$ T cells was higher than in SP_{IELs} and DP_{IELs}, although not significantly. Glucose uptake in naïve $CD4^+$ T cells was higher than in IEL cells. Among IELs, glucose uptake was increased in $TCR\gamma\delta^+$ T cells compared with $CD8\alpha\beta^+$ T cells, SP_{IELs}, and DP_{IELs} (Figure 2C). These data indicate that induced IELs exhibit reduced oxygen consumption, glycolysis, and glucose uptake.

Given that $CD8^+$ IELs showed an increased number of mitochondria with altered lipid metabolism compared with naïve $CD4^+$ T cells (Konjar et al., 2018), we next counted the number and size of mitochondria in naïve $CD4^+$ T cells and induced IELs, SP_{IELs}, and DP_{IELs}. The total number of mitochondria was increased in SP_{IELs} and DP_{IELs} compared with naïve $CD4^+$ T cells (Figures 2D and 2E). Interestingly, DP_{IELs}

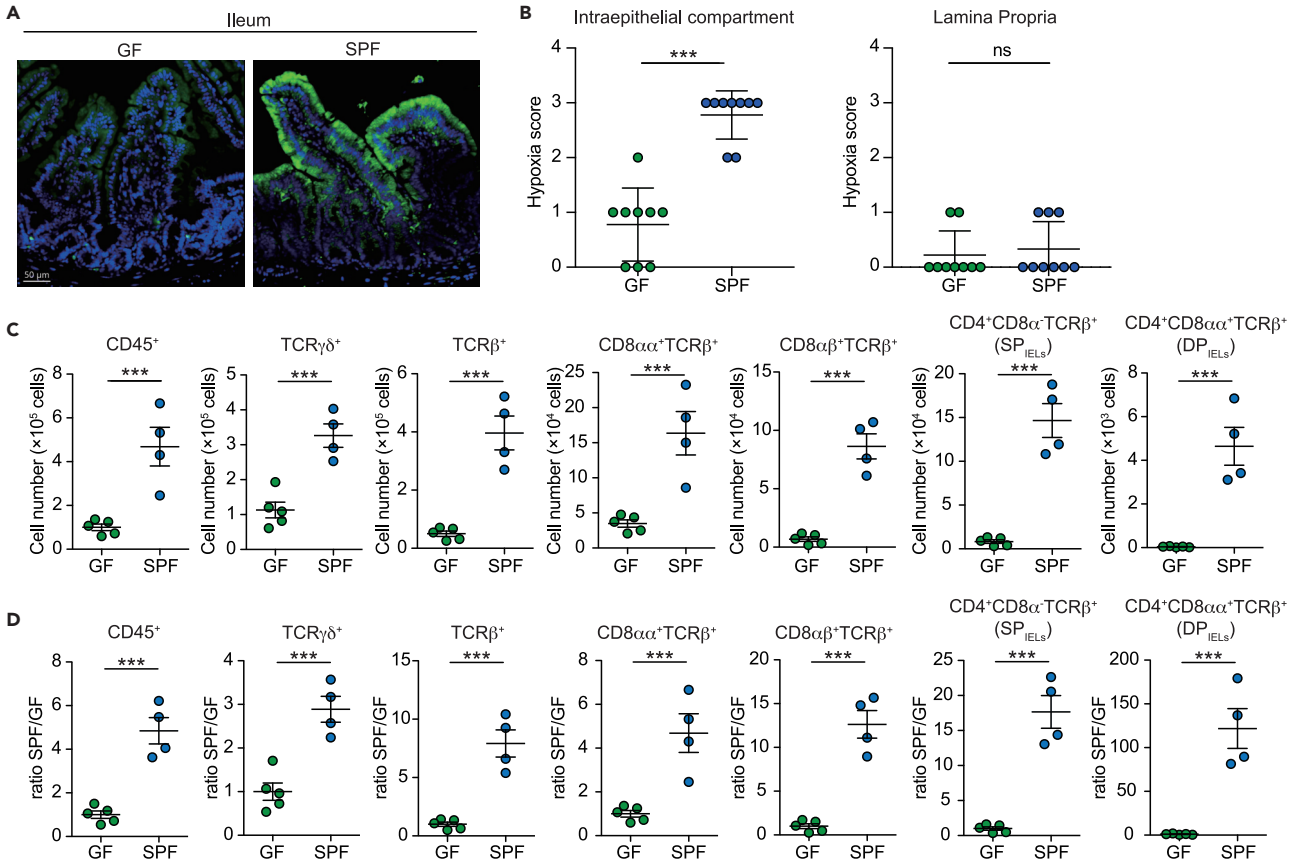

Figure 1. Intestinal intraepithelial compartment is hypoxic in SPF mice

(A) Immunohistochemical visualization (green) of "physiological hypoxia" in intestinal mucosa of wild-type mice by Hypoxyprobe-1 staining. Mice were administered pimonidazole 30 min before sacrifice. PFA-fixed small intestine samples were sectioned and stained according to the manufacturer's instructions and counterstained with DAPI.

(B) Epithelium and lamina propria regions were scored for intensity of hypoxia staining (0, no hypoxia; 1, mild focal hypoxia; 2, moderate multifocal hypoxia; 3, intense diffuse hypoxia). Each dot represents a hypoxia score of 9 individual images (n = 2 GF and n = 2 SPF).

(C and D) Percentage (C) and ratio between GF and SPF mice (D) of $CD45^+$, $TCR\gamma\delta^+$, $TCR\beta^+$, $CD8\alpha\alpha^+TCR\beta^+$, $CD8\alpha\beta^+TCR\beta^+$, $CD4^+CD8\alpha^-TCR\beta^+$ (SP_{IELs}), and $CD4^+CD8\alpha\alpha^+TCR\beta^+$ (DP_{IELs}) cells in small intestine epithelium. Data are expressed as mean ± SD of individual mice (n = 5 GF and n = 4 SPF). Results represent one of two independent experiments. ns: not significant, ***$p < 0.001$ (unpaired Student's *t* test with Welch's correction).

displayed a higher number of mitochondria than SP_{IELs}. Of note, the area of each mitochondrion in DP_{IELs} was smaller than in naïve $CD4^+$ T cells and SP_{IELs} (Figures 2D and 2F). Mitochondrial fission controls the number and the size of mitochondria in memory T cells (Buck et al., 2016). To support our findings, we analyzed the mitochondrial fission-related genes dynamin-related protein 1 (*Drp1*) and mitochondria fission 1 gene (*Fis1*). The expression levels of *Drp1* and *Fis1* were increased in SP_{IELs} and DP_{IELs} compared with naïve $CD4^+$ T cells (Figure 2G). The expression levels of *Drp1* and *Fis1* were comparable in DP_{IELs} and SP_{IELs}. These data indicate that SP_{IELs} and DP_{IELs} have a lower OCR with an increased number of small mitochondria, and mitochondrial fission genes are upregulated in SP_{IELs} and DP_{IELs}.

$CD4^+CD8\alpha\alpha^+TCR\beta^+$ IELs are a mitochondrial membrane potential^{lo} population

We then measured mitochondrial size and membrane potential in SP_{IELs} and DP_{IELs} using MitoTracker. Among $CD4^+$ T cells in spleen and mesenteric lymph node (mLN) cells, $CD4^+CD62L^+$ cells were classified as mitochondria size^{hi} and membrane potential^{hi} (gated as Q1) populations, and $CD4^+CD44^+$ effector and memory cells were identified as mitochondria size^{hi} and membrane potential^{lo} (Q2) populations (Figure S1A). We analyzed the size and membrane potential of mitochondria in natural IELs and induced IELs from 12-week-old GF mice and SPF mice. Most $TCR\gamma\delta^+$ T cells were mitochondria size^{lo} and membrane potential^{lo} (Q4) compared with naïve $CD4^+$ T cells. Of note, the percentage of each fraction (Q1–4) in $TCR\gamma\delta^+$ T cells was not significantly different between GF and SPF mice (Figures 3A and 3B). Next, we

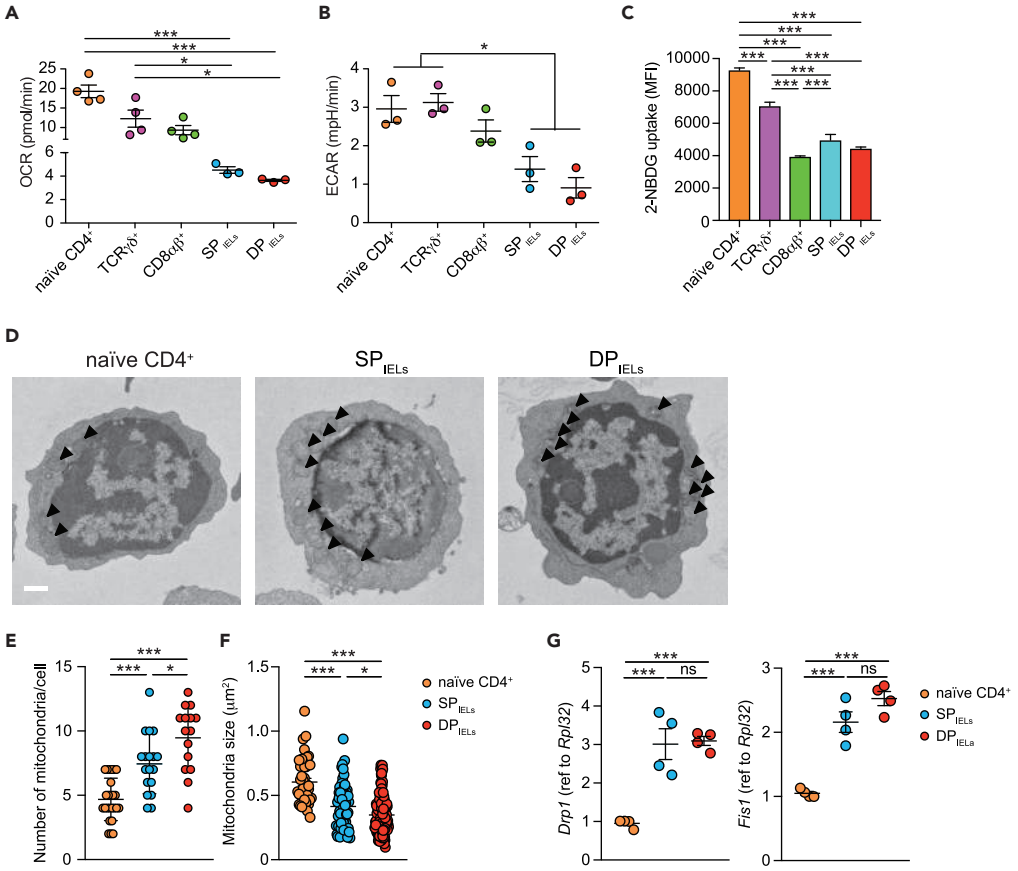

Figure 2. Induced CD4$^+$CD8αα$^+$TCRβ$^+$ IELs exhibit a reduced OCR and ECAR

(A and B) Summaries of the oxygen consumption rate (OCR) (A) and extracellular acidification rate (ECAR) (B) of TCRγδ$^+$, CD8αβ$^+$TCRβ$^+$, SP$_{IELs}$ (CD4$^+$CD8α$^-$TCRβ$^+$), and DP$_{IELs}$ (CD4$^+$CD8αα$^+$TCRβ$^+$) cells in small intestine epithelium and naive CD4$^+$ (splenic naive CD4$^+$ T) cells isolated from wild-type mice.

(C) Quantification of glucose uptake into TCRγδ$^+$, CD8αβ$^+$TCRβ$^+$, SP$_{IELs}$, and DP$_{IELs}$ cells in small intestine epithelium and naïve CD4$^+$ T cells isolated from wild-type mice.

(D) Transmission electron microscopy (TEM) electron micrographs of sorted SP$_{IELs}$, DP$_{IELs}$ cells in small intestine epithelium and naïve CD4$^+$ T cells isolated from wild-type mice. Black arrows indicate each mitochondrion. Results represent two independent experiments. Scale bar, 0.5 μm.

(E and F) Quantitation of TEM micrographs of sorted SP$_{IELs}$, DP$_{IELs}$ in small intestine epithelium and naïve CD4 T$^+$ cells isolated from wild-type mice showing difference in the number (E) (n = 15 to 25) and size (F) (n = 40 to 118) of the mitochondria.

(G) The mRNA level of *Drp1* and *Fis1* were evaluated by RT-qPCR with sorted fresh SP$_{IELs}$ and DP$_{IELs}$ in small intestine epithelium and naïve CD4$^+$ cells of wild-type mice (n = 4). The data were shown as fold change normalized to naïve CD4$^+$ T cells. Results represent one of two independent experiments. ns: not significant, *p < 0.05, **p < 0.01, ***p < 0.001 (one-way ANOVA with Tukey's multiple comparisons).

measured the mitochondrial size and membrane potential of CD4$^+$ T cells in the intraepithelial (CD4$_{IELs}$) and lamina propria (CD4$_{LPLs}$) compartment. The percentage of Q1 and Q3 in CD4$_{IELs}$ of SPF mice was reduced compared with GF mice, whereas the percentage of Q1 and Q3 in CD4$_{LPLs}$ was comparable between SPF mice and GF mice (Figures 3C–3F). In CD4$_{LPLs}$, the percentage of Q2 was slightly increased in GF mice than in SPF mice. These data indicate that CD4$_{IELs}$ but not CD4$_{LPLs}$ have a lower mitochondrial potential in SPF mice compared with GF mice. We then divided CD4$_{IELs}$ into two populations (SP$_{IELs}$ and DP$_{IELs}$) because DP$_{IELs}$ were increased in SPF mice (Figures 1C and 1D). The percentage of Q1 and Q2 in DP$_{IELs}$ was decreased compared with that in SP$_{IELs}$ (Figures 3G and 3H). We also confirmed that DP$_{IELs}$ exhibited a reduced mitochondrial membrane potential compared with SP$_{IELs}$ by tetramethylrhodamine ethyl ester (TMRE) staining (Figures 3I and 3J). Taken together, induced IELs, especially DP$_{IELs}$, are a population of cells with small mitochondria and low mitochondrial membrane potential.

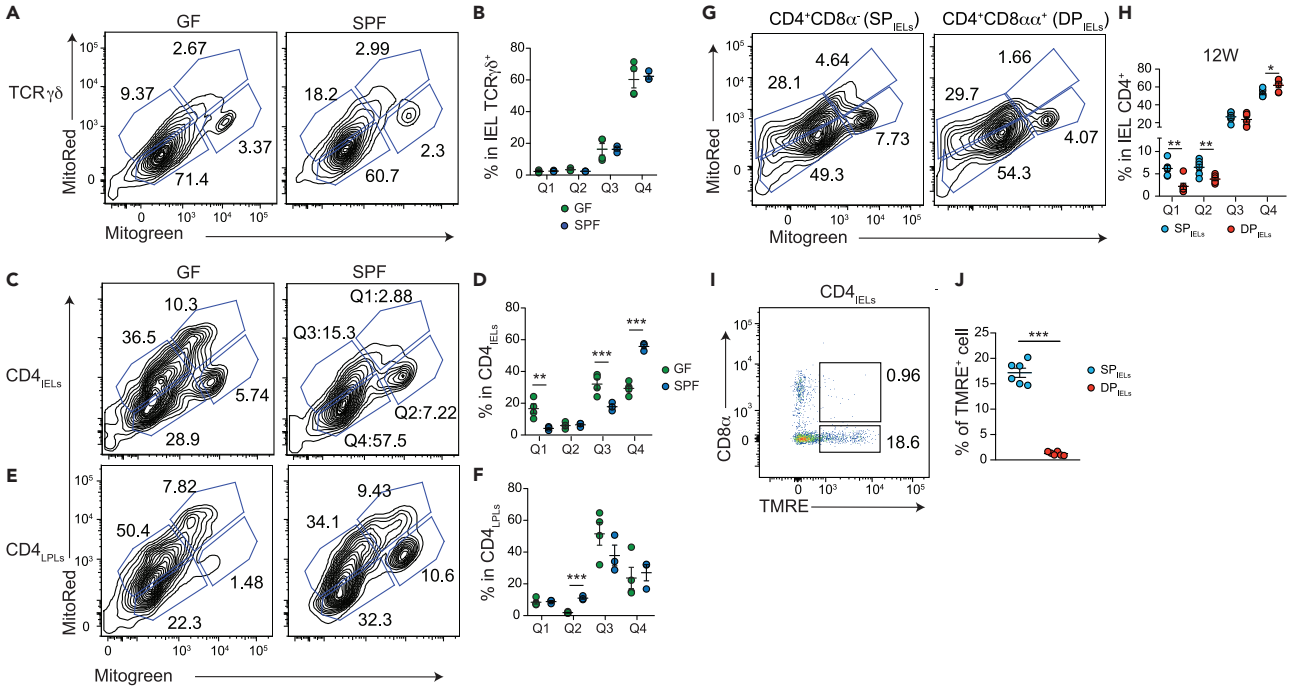

Figure 3. Induced CD4$^+$CD8αα$^+$TCRβ$^+$ IELs are a mitochondrial membrane potential^{lo} population

(A and B) Flow cytometric analysis of mitochondrial membrane potential and size monitored by MitoTracker staining (A) and frequencies of Q1, Q2, Q3, and Q4 on TCRγδ+ cells (B) among CD45$^+$ cells from small intestine epithelium of GF or SPF mice.

(C–F) Representative flow cytometric analysis and frequencies Q1, Q2, Q3, and Q4 of mitochondrial membrane potential and size monitored by MitoTracker staining of $CD4_{IELs}$ (C and D) and $CD4_{LPLs}$ (E and F) of wild-type mice reared under GF (n = 4) or SPF (n = 4) condition.

(G and H) Representative flow cytometric analysis (G) and frequencies Q1, Q2, Q3, and Q4 (H) of MitoTracker staining of SP_{IELs} and DP_{IELs} cells from 12W wild-type mice. n = 5.

(I and J) Representative flow cytometric analysis (I) and frequencies (J) of TMRE positive cells in SP_{IELs} and DP_{IELs} cells from small intestine epithelium of 12W wild-type mice. Data are composed of triplicate analysis from individual 2 mice. *p < 0.05, **p < 0.01, ***p < 0.001 (one-way ANOVA with Tukey's multiple comparisons for B, D, F, and H; unpaired Student's *t* test with Welch's correction for J).

2DG inhibits the induction of CD4$^+$CD8αα$^+$TCRβ$^+$ IELs

Because DP_{IELs} consume less glucose than naïve CD4$^+$ T cells (Figure 2C), we next investigated whether glucose uptake affects the development of DP_{IELs}. We administered 6-week-old mice with or without 2DG via daily intraperitoneal injection for 5 weeks (Figure 4A) (Hamanaka and Chandel, 2012). 2DG administration did not reduce the percentage of TCRγδ$^+$ T cells in CD45$^+$ cells but reduced the percentage of TCRβ$^+$ T cells in CD45$^+$ cells which contained the DP_{IELs} cells (Figure S2A). Among TCRβ$^+$ T cells, the percentage of CD8α$^+$CD8β$^-$ T cells was slightly increased in 2DG mice and the percentage of CD8αβ$^+$ T cells was comparable between with or without 2DG administration. Of note, the percentage of total CD4$^+$ T cells in TCRβ$^+$ T cells was reduced in 2DG administration. The proportion of DP_{IELs} among total CD4$^+$ cells before 2DG treatment was approximately 20%. The percentage of DP_{IELs} was ~40% without 2DG treatment and decreased to ~20% in 2DG treated mice (Figures 4B and 4C). Moreover, the percentage of DP_{IELs} in total TCRβ$^+$ cells and CD45$^+$ cells was decreased with 2DG treatment (Figure S2B).

These data indicate that 2DG inhibited the development of DP_{IELs}. 2DG might affect Treg populations because some ex-Tregs differentiate into DP_{IELs}. However, the percentages of Tregs were comparable between mice with and without 2DG (Figure 4D). These data indicate that 2DG inhibits the development of DP_{IELs} without changing the Treg population. To exclude the possibility of other immune cells being involved, we then questioned the oxygen concentration and 2DG directly affecting the development of DP_{IELs}. We cultured splenic naïve CD4$^+$ T cells with or without 2DG in the presence of TGF-β, retinoic acid (RA), and IFN-γ (DP_{IEL} condition) *in vitro* under normoxic (O_2 20%) or hypoxic conditions (O_2 8%) (Figures 4E–4G). As expected, the proportion of CD4$^+$CD8αα$^+$ T cells in total CD4$^+$ T cells was increased under the hypoxic condition compared with normoxia. These data indicate the hypoxia induces CD4$^+$CD8αα$^+$ T cells in DP_{IEL} condition *in vitro*. 2DG decreased the proportion of CD4$^+$CD8αα$^+$ T cells in CD4$^+$ T cells

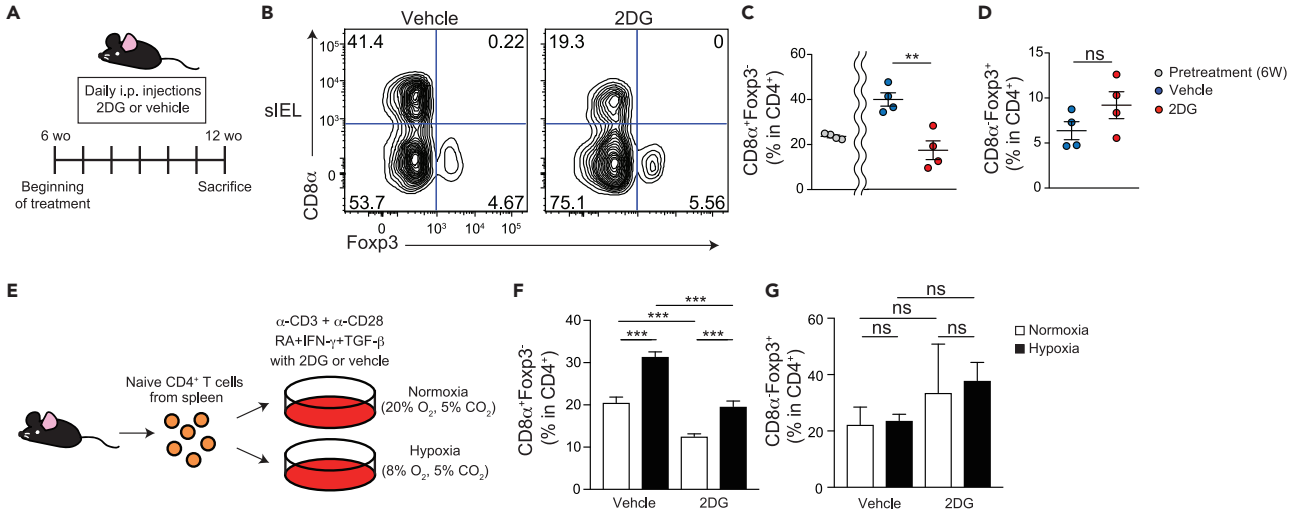

Figure 4. 2DG inhibits the induction of CD4$^+$CD8αα$^+$TCRβ$^+$ IELs

(A) Schematic diagram showing the experimental design to investigate the effect of 2DG treatment on wild-type mice *in vivo*.

(B–D) Representative flow cytometric figures of surface CD8α and intracellular Foxp3 (B) and frequencies of CD8α$^+$Foxp3$^-$ (C) and CD8α$^-$Foxp3$^+$ cells (D) among TCRβ$^+$CD4$^+$CD8β$^-$ T cells in small intestine epithelium from wild-type mice treated with or without 2DG via daily intraperitoneal injection for 5 weeks. Data are expressed as mean ± SD of individual mice (n = 4), representative of two independent experiments.

(E) Schematic diagram showing the experimental design to investigate the effect of 2DG treatment and hypoxic condition on development of naïve CD4$^+$ T cells into CD4$^+$CD8αα$^+$ cells *in vitro*.

(F and G) Frequencies of CD8α$^+$Foxp3$^-$ (F) and CD8α$^-$Foxp3$^+$ cells (G) among TCRβ$^+$CD4$^+$CD8β$^-$ cells after *in vitro* CD4$^+$CD8αα$^+$ cell induction in normoxic and hypoxic condition with or without 2DG treatment. Splenic naïve CD4$^+$ T cells isolated from wild-type mice are cultured for 4 days with plate-bound α-CD3 and α-CD28 in the presence of TGF-β+RA + IFN-γ. ns: not significant, **p < 0.01, ***p < 0.001 (unpaired Student's *t* test with Welch's correction).

when they cultured under both normoxic and hypoxic condition. Of note, 2DG tends to increase the proportion of Tregs in CD4$^+$ T cells in DP$_{IEL}$ condition but not significantly under both normoxic and hypoxic conditions. These data indicate that the prevention of glucose uptake inhibits the development of DP$_{IELs}$, and they consume less glucose than naïve CD4$^+$ T cells.

Hif1α/Hif2α are reduced during the development of CD4$^+$CD8αα$^+$TCRβ$^+$ IELs

The intestinal epithelium is an oxygen-poor environment with no blood vessels separating anaerobic intestinal bacteria from the intestinal epithelium. Hif1α and Hif2α are known to be upregulated under hypoxic conditions. We questioned whether the expression of HIF was upregulated in CD4$_{IELs}$. We FACS sorted naïve CD4$^+$ T cells, SP$_{IELs}$, and DP$_{IELs}$ and analyzed the expression of HIF-related genes (Figure 5A). As previously reported, DP$_{IELs}$ expressed higher levels of *Runx3* than SP$_{IELs}$ and naïve CD4$^+$ T cells. Interestingly, the RNA expression levels of *Hif1α* and *Hif2α* in DP$_{IELs}$ were lower than in SP$_{IELs}$. Von Hippel–Lindau (*Vhl*) is a negative regulator of HIF. The RNA expression level of *Vhl* was comparable between DP$_{IELs}$ and SP$_{IELs}$. These data indicate that DP$_{IELs}$ exhibit reduced *Hif1α*/*Hif2α* expression during development.

Hif/Vhl gene expression regulates the development of CD4$^+$CD8αα$^+$TCRβ$^+$ IELs

We next questioned whether the downregulation of *Hif1α*/*Hif2α* expression was essential for the development of DP$_{IELs}$. We crossed *Hif1α*$^{fl/fl}$*Hif2α*$^{fl/fl}$ mice with *Cd4*^{cre} mice to generate mice lacking *Hif1α* and *Hif2α* in CD4$^+$ T cells (Hif$^{\Delta CD4}$). The total number of IELs in Hif$^{\Delta CD4}$ mice was not increased compared with *Hif1α*$^{fl/fl}$*Hif2α*$^{fl/fl}$ mice (Figure S3A). The percentage of DP$_{IELs}$ was increased by almost 2-fold in Hif$^{\Delta CD4}$ mice compared with *Hif1α*$^{fl/fl}$*Hif2α*$^{fl/fl}$ mice, whereas the percentage of Tregs was decreased in Hif$^{\Delta CD4}$ mice compared with *Hif1α*$^{fl/fl}$*Hif2α*$^{fl/fl}$ mice (Figures 5B and 5C). As HIF1α also regulates retinoic acid-related orphan receptor gamma t (RORγt) expression (Shi et al., 2011), we confirmed that the proportion of RORγt$^+$Foxp3$^-$ IELs was decreased in Hif$^{\Delta CD4}$ mice compared with *Hif1α*$^{fl/fl}$*Hif2α*$^{fl/fl}$ mice (Figures S3B and S3C). Among LPLs, the percentages of Tregs and RORγt$^+$ Foxp3$^-$ T cells were comparable between Hif$^{\Delta CD4}$ mice and *Hif1α*$^{fl/fl}$*Hif2α*$^{fl/fl}$ mice (Figures S3D and S3E). These data indicate that the downregulation of *Hif1α*/*Hif2α* expression in CD4 T cells induces DP$_{IELs}$. Then, we crossed *Vhl*$^{fl/fl}$ mice with *Cd4*^{cre} mice to generate *Cd4*^{cre}:*Vhl*$^{fl/fl}$ (Vhl$^{\Delta CD4}$) mice and analyzed the cell populations at the age of 12 weeks. The percentage and total number of CD4$^+$ T cells in the thymus were comparable in *Vhl*$^{fl/fl}$ mice and Vhl$^{\Delta CD4}$

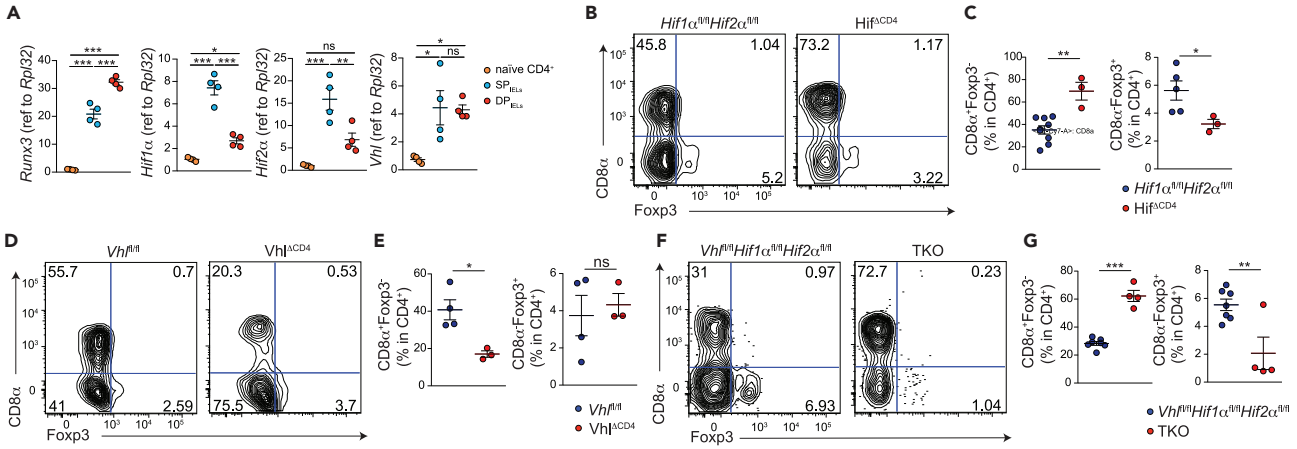

Figure 5. Hif/Vhl gene expression regulates the development of CD4$^+$CD8αα+TCRβ+ IELs

(A) The mRNA level of Runx3, Hif1α, Hif2α and Vhl were evaluated by RT-qPCR with sorted fresh naïve CD4$^+$ T cells from spleen and SPIELs, DPIELs cells from small intestine epithelium of wild-type mice (n = 4). The data were shown as fold change normalized to naïve CD4$^+$ T cells.

(B and C) Representative flow cytometric analysis of surface CD8α and intracellular Foxp3 (B) and frequencies of CD8α$^+$Foxp3$^-$ and CD8α$^-$Foxp3$^+$ cells (C) among TCRβ$^+$CD4$^+$CD8β$^-$ T cells in small intestine epithelium from *Hif1α*$^{fl/fl}$*Hif2α*$^{fl/fl}$ and *Cd4*^{cre}*Hif1α*$^{fl/fl}$*Hif2α*$^{fl/fl}$ (Hif$^{\Delta CD4}$) mice. Data are expressed as mean ± SD of individual mice (n = 3 to 9), representative of two independent experiments.

(D and E) Representative flow cytometric analysis of surface CD8α and intracellular Foxp3 (D) and frequencies of CD8α$^+$Foxp3$^-$ and CD8α$^-$Foxp3$^+$ cells (E) among TCRβ$^+$CD4$^+$CD8β$^-$ T cells in small intestine epithelium from *Vhl*$^{fl/fl}$ and *Cd4*^{cre}*Vhl*$^{fl/fl}$ (Vhl$^{\Delta CD4}$) mice. Data are expressed as mean ± SD of individual mice (n = 3 to 4), representative of two independent experiments.

(F and G) Representative flow cytometric analysis of surface CD8α and intracellular Foxp3 (F) and frequencies of CD8α$^+$Foxp3$^-$ and CD8α$^-$Foxp3$^+$ cells (G) among TCRβ$^+$CD4$^+$CD8β$^-$ T cells in small intestine epithelium from *Hif1α*$^{fl/fl}$*Hif2α*$^{fl/fl}$*Vhl*$^{fl/fl}$ and *Cd4*^{cre}*Hif1α*$^{fl/fl}$*Hif2α*$^{fl/fl}$*Vhl*$^{fl/fl}$ (TKO) mice. Data are expressed as mean ± SD of individual mice (n = 4 to 7), representative of two independent experiments. ns: not significant, *p < 0.05, **p < 0.01, ***p < 0.001 (one-way ANOVA with Tukey's multiple comparisons for A; unpaired Student's *t* test with Welch's correction for C, E, and G).

mice (Figures S4A–S4C), as previously reported (Zhu et al., 2019). The total number of CD4$^+$ T cells in IELs was also comparable in *Vhl*$^{fl/fl}$ mice and Vhl$^{\Delta CD4}$ mice (Figure S4D). As expected, the proportion of DP$_{IELs}$ but not Tregs was decreased in Vhl$^{\Delta CD4}$ mice compared with *Vhl*$^{fl/fl}$ mice (Figures 5D and 5E). We also found that the percentages of RORγt$^+$Foxp3$^-$ IELs and LPLs were increased in Vhl$^{\Delta CD4}$ mice (Figures S4E–S4H). These data indicate that the downregulation of *vhl* expression in CD4$^+$ T cells inhibits the development of DP$_{IELs}$. Because *Vhl* regulates *Hif1α/Hif2α* and vice versa, we further investigated whether *Hif1* or *Vhl* was important for the induction of DP$_{IELs}$ by crossing *Vhl*$^{fl/fl}$/*Hif1α*$^{fl/fl}$/*Hif2α*$^{fl/fl}$ mice with *Cd4*^{cre} mice [referred to as triple KO (TKO) mice]. Interestingly, TKO mice showed an increased proportion of DP$_{IELs}$ compared with *Vhl*$^{fl/fl}$/*Hif1α*$^{fl/fl}$/*Hif2α*$^{fl/fl}$ mice, similar to Hif$^{\Delta CD4}$ mice (Figures 5F and 5G). Taken together, these data suggest that the downregulation of *Hif1α/Hif2α* expression in CD4$^+$ T cells regulates the development of DP$_{IELs}$.

CD4$^+$CD8αα$^+$TCRβ$^+$ IELs show reduced phosphorylation level of S6 compared with CD4$^+$CD8α$^-$TCRβ$^+$ IELs

As DP$_{IELs}$ exhibit reduced *Hif1α/Hif2α* expression during development, and the downregulation of *Hif1α/Hif2α* expression is important for the development of DP$_{IELs}$, we hypothesized that the downregulation of *Hif1α/Hif2α* expression in CD4$_{IELs}$ is not only regulated by hypoxia but also by mTORC signaling, which controls *Hif1α/Hif2α* expression. mTORC exists as mTORC1 and mTORC2 complexes. Interestingly, although the expression of *Hif1α/Hif2α* was reduced in DP$_{IELs}$ compared with SP$_{IELs}$, the expression of the mTORC1 gene *Rptor* in DP$_{IELs}$ was comparable to that in SP$_{IELs}$ (Figure 6A). Both DP$_{IELs}$ and SP$_{IELs}$ expressed higher levels of *Rptor* than splenic naive CD4$^+$ T cells. We then analyzed the RNA expression of *Rptor*-related genes, including isoform 2 of the glycolytic enzyme hexokinase (*Hk2*) (enhances glucose metabolism) and arginase-2 (*Arg2*) (regulates L-arginine in the urea cycle). The expression of *Hk2* in DP$_{IELs}$ was slightly but not significantly increased compared with SP$_{IELs}$. The expression of *Arg2* was comparable in DP$_{IELs}$ and SP$_{IELs}$. The expression of *Rictor* was also comparable in DP$_{IELs}$ and SP$_{IELs}$. In addition, mTORC regulates sterol regulatory binding protein (SREBP), which mediates fatty acid metabolism. The expression of *Srebp1* and *Srebp2* in DP$_{IELs}$ was higher than in naïve CD4$^+$ T cells and SP$_{IELs}$ (Figure 6A). These data indicate that the expression level of mTORC in DP$_{IELs}$ was comparable to that in SP$_{IELs}$. However, DP$_{IELs}$ displayed

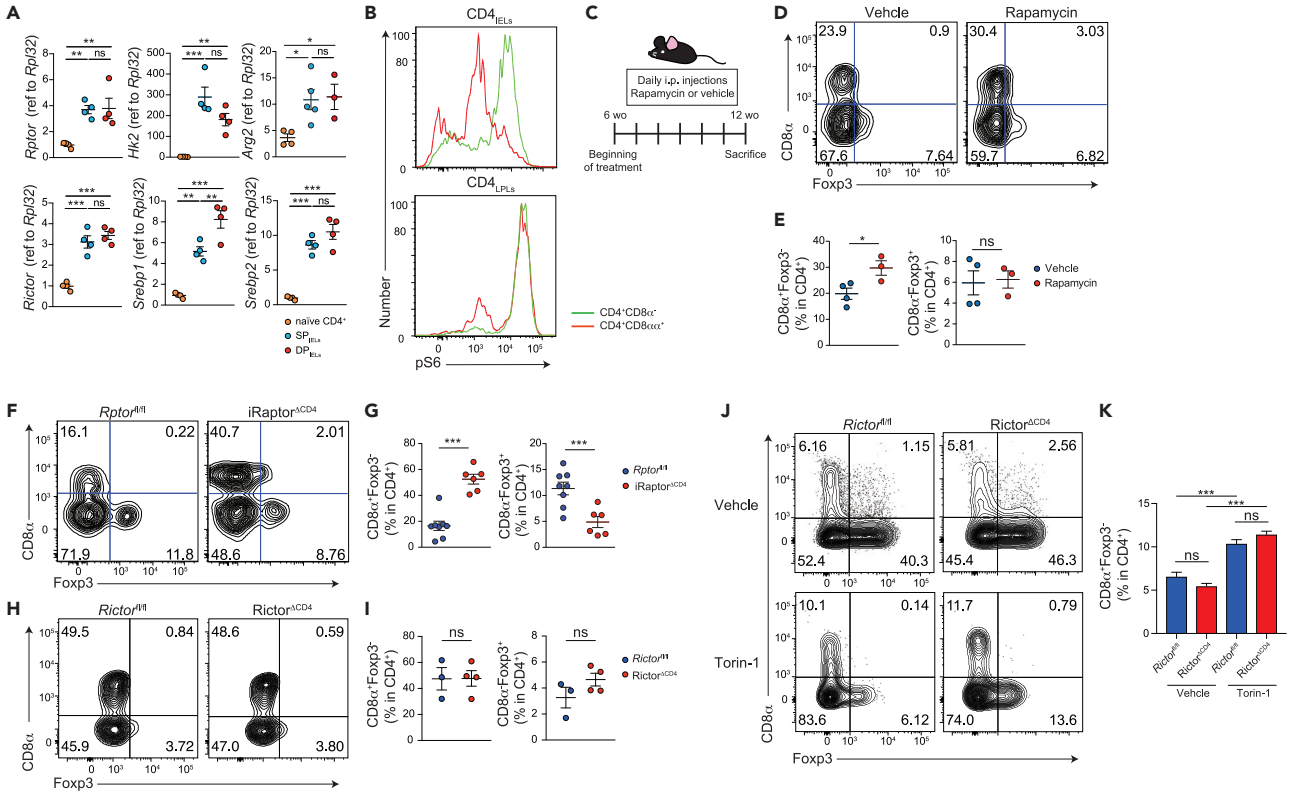

Figure 6. Downregulation of Rptor but not Rictor induces CD4$^+$CD8αα+TCRβ+ IELs

(A) The mRNA level of *Rptor, Hk2, Arg2, Rictor, Srebp1,* and *Srebp2* were evaluated by RT-qPCR with sorted fresh SP_{IELs} and DP_{IELs} in small intestine epithelium and naïve CD4$^+$ cells of wild-type mice (n = 4). The data were shown as fold change normalized to naïve CD4$^+$ T cells.

(B) Histogram demonstrating phosphorylation of S6 ribosomal protein in CD4$^+$CD8α$^-$ and CD4$^+$CD8αα$^+$ within CD4$^+$ cells from small intestine epithelium ($CD4_{IELs}$) or lamina propria ($CD4_{LPLs}$) compartment of wild-type mice. A representative of two independent experiments.

(C) Schematic diagram showing the experimental design to investigate the effect of Rapamycin treatment on wild-type mice *in vivo*.

(D and E) Representative flow cytometric figures of surface CD8α and intracellular Foxp3 (D) and frequencies of CD8α$^+$Foxp3$^-$ and CD8α$^-$Foxp3$^+$ cells (E) among TCRβ$^+$CD4$^+$CD8β$^-$ T cells in small intestine epithelium from wild-type mice treated with or without Rapamycin via intraperitoneal injection for 5 weeks. Data are expressed as mean ± SD of individual mice (n = 3 to 9), representative of two independent experiments.

(F and G) Representative flow cytometric figures of surface CD8α and intracellular Foxp3 (F) and frequencies of CD8α$^+$Foxp3$^-$ and CD8α$^-$Foxp3$^+$ cells (G) among TCRβ$^+$CD4$^+$CD8β$^-$ T cells in small intestine epithelium from *Rptor*$^{fl/fl}$ and *Cd4*^{cre}*Rptor*$^{fl/fl}$ (iRaptor$^{\Delta CD4}$) treated with tamoxifen via oral administration for 5 weeks. Data are expressed as mean ± SD of individual mice (n = 3 to 9), representative of two independent experiments.

(H and I) Representative flow cytometric figures of surface CD8α and intracellular Foxp3 (H) and frequencies of CD8α$^+$Foxp3$^-$ and CD8α$^-$Foxp3$^+$ cells (I) among TCRβ$^+$CD4$^+$CD8β$^-$ T cells in small intestine epithelium from *Rictor*$^{fl/fl}$ and *Cd4*^{cre}*Rictor*$^{fl/fl}$ (Rictor$^{\Delta CD4}$) mice. Data are expressed as mean ± SD of individual mice (n = 4), representative of two independent experiments.

(J and K) Representative flow cytometric figures of surface CD8α and intracellular Foxp3 (J) and frequencies of CD8α$^+$Foxp3$^-$ (K) cells among TCRβ$^+$CD4$^+$CD8β$^-$ cells after *in vitro* CD4$^+$CD8αα$^+$ cell induction with or without Torin 1 treatment. Naïve CD4$^+$ T cells isolated from Rictor$^{\Delta CD4}$ mice are cultured for 4 days with plate-bound α-CD3 and α-CD28 in the presence of TGF-β+RA + IFN-γ. ns: not significant, *p < 0.05, **p < 0.01, ***p < 0.001 (one-way ANOVA with Tukey's multiple comparisons for A and K; unpaired Student's *t* test with Welch's correction for E, G, and I).

reduced *Hif1α/Hif2α* and increased *Srebp1* and *Srebp2* expression. Given that T cell receptor signaling induces the Akt/mTOR/pS6 pathway, we next analyzed pS6 in $CD4_{IELs}$. DP_{IELs} expressed lower phosphorylation levels of S6 than SP_{IELs} (Figure 6B). Of note, CD4$^+$CD8αα$^+$ LPLs and CD4$^+$CD8α$^-$ LPLs expressed similar levels of pS6. Our findings are consistent and show reduced mTORC/pS6 signaling in DP_{IELs}.

Downregulation of *Rptor* but not *rictor* induces CD4$^+$CD8αα$^+$TCRβ$^+$ IELs

We next questioned whether mTORC1 or 2 was important for the induction of DP_{IELs}. We first administered rapamycin, which modulates mTORC1 signaling, to 6-week-old mice for 5 weeks (Figure 6C) (Neff et al., 2013). Interestingly, the percentage of DP_{IELs} was increased in mice treated with rapamycin compared with control mice, whereas the percentages of Tregs in IEL were comparable in both groups (Figures 6D and 6E). The percentage and total number of Rorγt$^+$Foxp3$^-$ cells in LPL were decreased in rapamycin-treated mice, whereas the

percentage and total number of Rorγt^{-}Foxp3^{+} cells were increased in rapamycin-treated mice (Figures S5A and S5B). The total number of Rorγt^{-}Foxp3^{+} cells in rapamycin-treated mice was reduced, but the percentage was comparable. These data indicate that the inhibition of mTORC1 function is important for the development of DP_{IELs}. To confirm mTORC1 involvement in the induction of DP_{IELs}, we generated *Cd4*^{creERT2}:*Rptor*$^{fl/fl}$ (referred to as iRaptor$^{\Delta CD4}$) mice with CD4-specific *Rptor* downregulation after tamoxifen administration because the downregulation of *Rptor* in the thymus impairs peripheral CD4^{+} T cells (Hoshii et al., 2014). We administered tamoxifen to mice at the age of 6 weeks and analyzed them 5 weeks later. No spontaneous intestinal inflammation was observed in *Rptor*$^{fl/fl}$ or iRaptor$^{\Delta CD4}$ mice (data not shown). DP_{IELs} accounted for approximately 60% of $CD4_{IELs}$, and the proportion of DP_{IELs} was significantly increased in iRaptor$^{\Delta CD4}$ mice (Figures 6F and 6G). We then generated *Cd4*^{cre}:*Rictor*$^{fl/fl}$ mice (referred to as Rictor$^{\Delta CD4}$). The proportion of DP_{IELs} was comparable between *Rictor*$^{fl/fl}$ and Rictor$^{\Delta CD4}$ mice (Figures 6H and 6I). Moreover, we cultured naive CD4^{+} T cells from *Rictor*$^{fl/fl}$ mice and Rictor$^{\Delta CD4}$ mice under the DP_{IEL} condition with or without Torin 1. As observed *in vivo*, the percentage of DP_{IELs} in CD4^{+} T cells in the absence of Torin 1 was comparable between *Rictor*$^{fl/fl}$ and Rictor$^{\Delta CD4}$ cells *in vitro*. Torin 1 increased the percentage of DP_{IELs} development in both *Rictor*$^{fl/fl}$ and Rictor$^{\Delta CD4}$ cells (Figures 6J and 6K). Taken together, the inhibition of mTORC1 functionally but not mTORC2 is important for the development of DP_{IELs}, whereas the expression levels of *Rptor* and *Rictor* are not downregulated during the development of DP_{IELs}.

DISCUSSION

CD4-induced IELs, especially CD4^{+}CD8αα^{+} T cells, in the intestinal epithelium are not increased in GF mice, indicating that the involvement of bacteria in the intestinal epithelium plays a major role in the induction of CD4-induced IELs (Sujino et al., 2016). CD4^{+}CD8αα^{+} T cells are induced by aryl hydrocarbon receptor ligands from food or intestinal bacteria and the surrounding environment, such as IL-15, food antigens, and MHC class II molecules in the intestinal epithelium (Bilate et al., 2016; Mucida et al., 2013). Environmental cues shape induced IELs; however, how the cells adapt in oxygen rich or poor circumstances remains poorly understood. Similarly, how induced IELs adapt to their environmental conditions by altering gene expression related to intracellular metabolism is unknown (Almeida et al., 2016; Buck et al., 2015; Dumitru et al., 2018; Konjar et al., 2018; Phan et al., 2016; Raud et al., 2018; Shi et al., 2011). Induced $CD4_{IELs}$ exist as long-lived effector memory cells and express enzymes, such as granzyme B. Effector T cells are induced by elevated glycolysis, and they upregulate *Hif1α/Hif2α* expression. In contrast, memory T cells survive long-term in peripheral tissue by using OXPHOS. Here, we determined that induced $CD4_{IELs}$, especially DP_{IELs}, adapt to their unique metabolic conditions and exhibit a low OCR with reduced glucose uptake and anabolic glycolysis.

We first show that oxygen saturation is decreased in organs with poor blood flow, including the intestinal epithelium, not only because of cell oxygen consumption but also the presence of intestinal bacteria. Previously the number of TCRγδ^{+} cells was comparable in the GF and SPF conditions (Hoytema van Konijnenburg et al., 2017). As we counted the intestinal live cells in GF and SPF condition, we observed the increased number of both TCRγδ^{+} cells and TCRβ^{+} cells in SPF condition. Moreover, the total number of CD4^{+} T cells, especially DP_{IELs} T cells, increased dramatically In the SPF condition.

In the small intestine, the presence of several commensal anaerobes that consume oxygen is consistent with the results. Long-lived memory CD8^{+} T cells exhibit an increased mitochondrial size and membrane potential, resulting in a higher level of oxygen consumption (Buck et al., 2016). $CD4_{IELs}$ consume less oxygen with increased mitochondrial fission and low mitochondrial membrane potential during development. Some IELs show an increased mitochondrial size and membrane potential after anti-CD3 antibody injection (Konjar et al., 2018). Anti-CD3 antibodies induce severe inflammation in the small intestine. As a result, cells use mitochondrial respiration because the oxygen supply might be increased in the epithelial compartment of the small intestine. Because DP_{IELs} are diminished after anti-CD3 antibody injection, we cannot conclude that the size of mitochondria and membrane potential are increased in DP_{IELs} after anti-CD3 antibody stimulation. We demonstrate hypoxic conditions induce more CD4^{+}CD8αα^{+} T cells in DP_{IEL} condition *in vitro*. However, the effect of oxygen saturation itself on the differentiation and maintenance of $CD4_{IELs}$ remains to be investigated. Our data suggest that induced $CD4_{IELs}$ are the population of cells that adapt to the hypoxic intraepithelial compartment.

DP_{IELs} display enhanced gene expression of mTORC, which regulate HIF, mitochondrial biosynthesis, and lipid metabolism. However, DP_{IELs} exhibit reduced HIF and pS6 expression during development, which are

downstream factors of mTORC. Although DP_{IELs} reduce glucose uptake compared with naïve $CD4^+$ T cells, complete prevention of glucose intake with 2DG did not increase DP_{IELs}, indicating that glucose intake is indispensable for the development of DP_{IELs}.

DP_{IELs} do not show an increase in NUR77, indicating reduced T cell receptor signaling, but they express TCRβ (Bilate et al., 2020). In addition, previous studies have shown that MHC-II signaling in the epithelium is required for the induction of DP_{IELs} but dispensable for their expansion (Bilate et al., 2020; Mucida et al., 2013). Once naïve $CD4^+$ T cells activated via T cell receptor signaling import glucose, T cell activation continues in the late phase via Akt/pS6 and HIF upregulation with increased glucose uptake (Frauwirth et al., 2002; Jacobs et al., 2008; Menk et al., 2018). Interestingly, DP_{IELs} show reduced pS6 expression, HIF, and glucose uptake during their development from SP_{IELs}. Thus, DP_{IELs} might develop from cells that are activated temporally and quickly adapt to the tissue environments by reducing the expression of pS6 and HIF.

DP_{IELs} display reduced pS6 signaling and Hif1α expression but not decreased mTORC expression during their development from SP_{IELs}. The downregulation of mTORC1 or HIF in $CD4^+$ T cells induces more DP_{IELs}. These data indicate that mTORC gene expression in DP_{IELs} may play a role other than regulating glucose uptake or HIF. One possibility is that memory T cells residing in the peripheral tissue consume fatty acids (Fahrer et al., 2001; Konkel et al., 2011; Pan et al., 2017). Therefore, mTORC in DP_{IELs} might regulate lipid metabolism. In fact, the expression levels of the lipid biosynthesis genes *Srebp1* and *Srebp2* were increased in DP_{IELs} compared with naïve $CD4^+$ T cells and SP_{IELs}. The mechanisms by which mTORC regulates the balance between HIF, glucose uptake, and lipid metabolism in SP_{IELs} and DP_{IELs} remain unknown.

Compared with *Hif2α*, *Hif1α* is dominantly expressed in $CD4^+$ T cells. *Hif1α* expression might be a key factor that regulates DP_{IELs}. The specific factor that reduces mTORC1 or HIF expression and promotes DP_{IELs} development is still unknown. Further studies are needed because we cannot exclude the possibility that environmental autocrine or paracrine signals, such as cytokine production by the downregulation of mTORC1 or hypoxia in $CD4^+$ T cells, might induce DP_{IELs}.

Here, we demonstrate that $CD4_{IELs}$ alter their metabolic status and express unique genes to adapt to hypoxic conditions, and the downregulation of *Rptor* or *Hif1α/Hif2α* expression induces DP_{IELs} (Figure S6). TCRγδ cells rapidly use glycolysis and migrate to protect the epithelium following bacterial invasion via MYD88 signaling. However, DP_{IELs}, which increase in number with aging, are dual function cells with the potential to suppress intestinal inflammation, produce IL-10, and prevent bacterial invasion (Bilate et al., 2020; Mucida et al., 2013). The presence of diverse cell populations dependent on various metabolic pathways and metabolic genes in the IEL may be significant in the intestinal epithelium, which is at the forefront of immune tolerance and immune responses against antigens.

Limitations of the study

We measure the OCR and ECAR in splenic naïve $CD4^+$ T cells and IELs. The OCR and ECAR in this study do not fully capture in each organ, because we analyze them after isolating each cell from peripheral tissue and the localization of each cell is different peripherally. We analyzed the frequencies and numbers of each immune cell in the intestine, but the right control of the metabolic study is not determined yet. DP_{IELs} are differentiated by transcriptional factors, such as *Runx3*, *Zbtb7b*, *Tbet* and by the environmental factors, such as IL-15 and IFN-γ produced by $CD4^+$ T cells or the other immune cells, but it is unknown how these transcriptional factor and environmental factors affect the metabolic status to develop DP_{IELs}. We measured mitochondrial size, membrane potential with fission related genes, but the mitochondrial content and the precise mechanism of mitochondrial fission related genes on DP_{IELs} are not elucidated yet.

STAR★METHODS

Detailed methods are provided in the online version of this paper and include the following:

- KEY RESOURCES TABLE
- RESOURCE AVAILABILITY
  - Lead contact
  - Materials availability
  - Data and code availability

SUPPLEMENTAL INFORMATION

Supplemental information can be found online at https://doi.org/10.1016/j.isci.2022.104021.

ACKNOWLEDGMENTS

This work was supported by Grants-in-Aid from the Japanese Society for the Promotion of Science (JSPS) (19K17503 to Y.H., 17K19668, 17H05082, 19K22624, 20H03665, 21K18272 to T.S., 19K08402 to N.H., 21H02905 to H.O., 21K07084 K.O.), the Japan Agency for Medical Research and Development (19ek0109214 to T.S., 21gm1510002h0001 to T.K.), Mochida Memorial Foundation (T.S.), Takeda Science Foundation (T.S.), GSK Science Foundation (T.S.), and Yakult Bioscience Research Foundation (T.S.). We thank Jeremy Allen, PhD, and Melissa Crawford, PhD, from Edanz (https://jp.edanz.com/ac) for editing a draft of this manuscript.

AUTHOR CONTRIBUTIONS

Y.H., E.N., K.M., and T.S. performed experiments. T.S. designed and supervised the experiments and wrote the manuscript. Y.Y., S.T., S.U., K.O., Y.M., N.N., K.T., N.H., and H.O. assisted with experiments. T.I., A.H., and Y.K. provided mice and assisted with generating mice. T.S. and T.K. conceived the paper.

DECLARATION OF INTERESTS

Kentaro Miyamoto is an employee of Miyarisan Pharm. The other authors declare no competing interests.

Received: May 3, 2021
Revised: January 28, 2022
Accepted: March 1, 2022
Published: April 15, 2022

REFERENCES

Almeida, L., Lochner, M., Berod, L., and Sparwasser, T. (2016). Metabolic pathways in T cell activation and lineage differentiation. Semin. Immunol. *28*, 514–524.

Angelin, A., Gil-de-Gomez, L., Dahiya, S., Jiao, J., Guo, L., Levine, M.H., Wang, Z., Quinn, W.J., 3rd, Kopinski, P.K., Wang, L., et al. (2017). Foxp3 reprograms T cell metabolism to function in low-glucose, high-lactate environments. Cell Metab *25*, 1282–1293.e1287.

Bilate, A.M., Bousbaine, D., Mesin, L., Agudelo, M., Leube, J., Kratzert, A., Dougan, S.K., Victora, G.D., and Ploegh, H.L. (2016). Tissue-specific emergence of regulatory and intraepithelial T cells from a clonal T cell precursor. Sci. Immunol. *1*, eaaf7471.

Bilate, A.M., London, M., Castro, T.B.R., Mesin, L., Bortolatto, J., Kongthong, S., Harnagel, A., Victora, G.D., and Mucida, D. (2020). T cell receptor is required for differentiation, but not maintenance, of intestinal CD4(+) intraepithelial lymphocytes. Immunity *53*, 1001–1014.

Buck, M.D., O'Sullivan, D., Klein Geltink, R.I., Curtis, J.D., Chang, C.H., Sanin, D.E., Qiu, J., Kretz, O., Braas, D., van der Windt, G.J., et al. (2016). Mitochondrial dynamics controls T cell fate through metabolic programming. Cell *166*, 63–76.

Buck, M.D., O'Sullivan, D., and Pearce, E.L. (2015). T cell metabolism drives immunity. J. Exp. Med. *212*, 1345–1360.

Cervantes-Barragan, L., Chai, J.N., Tianero, M.D., Di Luccia, B., Ahern, P.P., Merriman, J., Cortez, V.S., Caparon, M.G., Donia, M.S., Gilfillan, S., et al. (2017). Lactobacillus reuteri induces gut intraepithelial CD4(+)CD8alphaalpha(+) T cells. Science *357*, 806–810.

Cheroutre, H., Lambolez, F., and Mucida, D. (2011). The light and dark sides of intestinal intraepithelial lymphocytes. Nat. Rev. Immunol. *11*, 445–456.

Dodd, K.M., Yang, J., Shen, M.H., Sampson, J.R., and Tee, A.R. (2015). mTORC1 drives HIF-1alpha and VEGF-A signalling via multiple mechanisms involving 4E-BP1, S6K1 and STAT3. Oncogene *34*, 2239–2250.

Dumitru, C., Kabat, A.M., and Maloy, K.J. (2018). Metabolic adaptations of CD4(+) T cells in inflammatory disease. Front Immunol. *9*, 540. https://doi.org/10.3389/fimmu.2018.00540.

Fahrer, A.M., Konigshofer, Y., Kerr, E.M., Ghandour, G., Mack, D.H., Davis, M.M., and Chien, Y.H. (2001). Attributes of gammadelta intraepithelial lymphocytes as suggested by their transcriptional profile. Proc. Natl. Acad. Sci. U S A *98*, 10261–10266.

Frauwirth, K.A., Riley, J.L., Harris, M.H., Parry, R.V., Rathmell, J.C., Plas, D.R., Elstrom, R.L., June, C.H., and Thompson, C.B. (2002). The CD28 signaling pathway regulates glucose metabolism. Immunity *16*, 769–777.

Groux, H., O'Garra, A., Bigler, M., Rouleau, M., Antonenko, S., de Vries, J.E., and Roncarolo, M.G. (1997). A CD4+ T-cell subset inhibits antigen-specific T-cell responses and prevents colitis. Nature *389*, 737–742.

Gruber, M., Hu, C.J., Johnson, R.S., Brown, E.J., Keith, B., and Simon, M.C. (2007). Acute postnatal ablation of Hif-2alpha results in anemia. Proc. Natl. Acad. Sci. U S A *104*, 2301–2306.

Haase, V.H., Glickman, J.N., Socolovsky, M., and Jaenisch, R. (2001). Vascular tumors in livers with targeted inactivation of the von Hippel-Lindau tumor suppressor. Proc. Natl. Acad. Sci. U S A *98*, 1583–1588.

Hamanaka, R.B., and Chandel, N.S. (2012). Targeting glucose metabolism for cancer therapy. J. Exp. Med. *209*, 211–215.

He, L., Gomes, A.P., Wang, X., Yoon, S.O., Lee, G., Nagiec, M.J., Cho, S., Chavez, A., Islam, T., Yu, Y., et al. (2018). mTORC1 promotes metabolic reprogramming by the suppression of GSK3-dependent Foxk1 phosphorylation. Mol. Cell *70*, 949–960.e944.

Hoshii, T., Kasada, A., Hatakeyama, T., Ohtani, M., Tadokoro, Y., Naka, K., Ikenoue, T., Ikawa, T., Kawamoto, H., Fehling, H.J., et al. (2014). Loss of mTOR complex 1 induces developmental blockage in early T-lymphopoiesis and eradicates T-cell acute lymphoblastic leukemia cells. Proc. Natl. Acad. Sci. U S A *111*, 3805–3810.

Hoytema van Konijnenburg, D.P., Reis, B.S., Pedicord, V.A., Farache, J., Victora, G.D., and Mucida, D. (2017). Intestinal epithelial and intraepithelial T cell crosstalk mediates a dynamic response to infection. Cell *171*, 783–794.e713.

Jacobs, S.R., Herman, C.E., Maciver, N.J., Wofford, J.A., Wieman, H.L., Hammen, J.J., and Rathmell, J.C. (2008). Glucose uptake is limiting in T cell activation and requires CD28-mediated Akt-dependent and independent pathways. J. Immunol. *180*, 4476–4486.

Jung, J., Zeng, H., and Horng, T. (2019). Metabolism as a guiding force for immunity. Nat. Cell Biol *21*, 85–93.

Konjar, S., Frising, U.C., Ferreira, C., Hinterleitner, R., Mayassi, T., Zhang, Q., Blankenhaus, B., Haberman, N., Loo, Y., Guedes, J., et al. (2018). Mitochondria maintain controlled activation state of epithelial-resident T lymphocytes. Sci. Immunol. *3*, eaan2543.

Konkel, J.E., Maruyama, T., Carpenter, A.C., Xiong, Y., Zamarron, B.F., Hall, B.E., Kulkarni, A.B., Zhang, P., Bosselut, R., and Chen, W. (2011). Control of the development of CD8alphaalpha+ intestinal intraepithelial lymphocytes by TGF-beta. Nat. Immunol. *12*, 312–319.

MacIver, N.J., Michalek, R.D., and Rathmell, J.C. (2013). Metabolic regulation of T lymphocytes. Annu. Rev. Immunol. *31*, 259–283.

Magee, J.A., Ikenoue, T., Nakada, D., Lee, J.Y., Guan, K.L., and Morrison, S.J. (2012). Temporal changes in PTEN and mTORC2 regulation of hematopoietic stem cell self-renewal and leukemia suppression. Cell Stem Cell *11*, 415–428.

Menk, A.V., Scharping, N.E., Moreci, R.S., Zeng, X., Guy, C., Salvatore, S., Bae, H., Xie, J., Young, H.A., Wendell, S.G., et al. (2018). Early TCR signaling induces rapid aerobic glycolysis enabling distinct acute T cell effector functions. Cell Rep *22*, 1509–1521.

Mucida, D., Husain, M.M., Muroi, S., van Wijk, F., Shinnakasu, R., Naoe, Y., Reis, B.S., Huang, Y., Lambolez, F., Docherty, M., et al. (2013). Transcriptional reprogramming of mature CD4(+) helper T cells generates distinct MHC class II-restricted cytotoxic T lymphocytes. Nat. Immunol. *14*, 281–289.

Neff, F., Flores-Dominguez, D., Ryan, D.P., Horsch, M., Schroder, S., Adler, T., Afonso, L.C., Aguilar-Pimentel, J.A., Becker, L., Garrett, L., et al. (2013). Rapamycin extends murine lifespan but has limited effects on aging. J. Clin. Invest. *123*, 3272–3291.

Newton, R., Priyadharshini, B., and Turka, L.A. (2016). Immunometabolism of regulatory T cells. Nat. Immunol. *17*, 618–625.

Olivares-Villagomez, D., and Van Kaer, L. (2018). Intestinal intraepithelial lymphocytes: sentinels of the mucosal barrier. Trends Immunol. *39*, 264–275.

Pan, Y., Tian, T., Park, C.O., Lofftus, S.Y., Mei, S., Liu, X., Luo, C., O'Malley, J.T., Gehad, A., Teague, J.E., et al. (2017). Survival of tissue-resident memory T cells requires exogenous lipid uptake and metabolism. Nature *543*, 252–256.

Pearce, E.L., and Pearce, E.J. (2013). Metabolic pathways in immune cell activation and quiescence. Immunity *38*, 633–643.

Phan, A.T., Doedens, A.L., Palazon, A., Tyrakis, P.A., Cheung, K.P., Johnson, R.S., and Goldrath, A.W. (2016). Constitutive glycolytic metabolism supports CD8(+) T cell effector memory differentiation during viral infection. Immunity *45*, 1024–1037.

Raud, B., McGuire, P.J., Jones, R.G., Sparwasser, T., and Berod, L. (2018). Fatty acid metabolism in CD8(+) T cell memory: challenging current concepts. Immunol. Rev. *283*, 213–231.

Reis, B.S., Rogoz, A., Costa-Pinto, F.A., Taniuchi, I., and Mucida, D. (2013). Mutual expression of the transcription factors Runx3 and ThPOK regulates intestinal CD4(+) T cell immunity. Nat. Immunol. *14*, 271–280.

Ryan, H.E., Poloni, M., McNulty, W., Elson, D., Gassmann, M., Arbeit, J.M., and Johnson, R.S. (2000). Hypoxia-inducible factor-1alpha is a positive factor in solid tumor growth. Cancer Res. *60*, 4010–4015.

Shi, L.Z., Wang, R., Huang, G., Vogel, P., Neale, G., Green, D.R., and Chi, H. (2011). HIF1alpha-dependent glycolytic pathway orchestrates a metabolic checkpoint for the differentiation of TH17 and Treg cells. J. Exp. Med. *208*, 1367–1376.

Sujino, T., London, M., Hoytema van Konijnenburg, D.P., Rendon, T., Buch, T., Silva, H.M., Lafaille, J.J., Reis, B.S., and Mucida, D. (2016). Tissue adaptation of regulatory and intraepithelial CD4(+) T cells controls gut inflammation. Science *352*, 1581–1586.

Sydora, B.C., Mixter, P.F., Holcombe, H.R., Eghtesady, P., Williams, K., Amaral, M.C., Nel, A., and Kronenberg, M. (1993). Intestinal intraepithelial lymphocytes are activated and cytolytic but do not proliferate as well as other T cells in response to mitogenic signals. J. Immunol. *150*, 2179–2191.

Van Kaer, L., and Olivares-Villagomez, D. (2018). Development, homeostasis, and functions of intestinal intraepithelial lymphocytes. J. Immunol. *200*, 2235–2244.

Vandereyken, M., James, O.J., and Swamy, M. (2020). Mechanisms of activation of innate-like intraepithelial T lymphocytes. Mucosal Immunol. *13*, 721–731.

Yu, S., Bruce, D., Froicu, M., Weaver, V., and Cantorna, M.T. (2008). Failure of T cell homing, reduced CD4/CD8alphaalpha intraepithelial lymphocytes, and inflammation in the gut of vitamin D receptor KO mice. Proc. Natl. Acad. Sci. U S A *105*, 20834–20839.

Zhu, Y., Zhao, Y., Zou, L., Zhang, D., Aki, D., and Liu, Y.C. (2019). The E3 ligase VHL promotes follicular helper T cell differentiation via glycolytic-epigenetic control. J. Exp. Med. *216*, 1664–1681.

STAR★METHODS

KEY RESOURCES TABLE

REAGENT or RESOURCE	SOURCE	IDENTIFIER
Antibodies		
CD4 (clone: RM4-5; BV421)	Biolegend	Cat# 100544; RRID: AB_11219790
CD8α (clone: 53-6.7; PE-Cy7)	BD Bioscience	Cat# 552877; RRID: AB_394506
CD8β (clone: eBioH35-17.2; APC)	eBioscience	Cat# 17-0083-81; RRID: AB_657760
CD44 (clone: IM7; APC)	Biolegend	Cat# 103012; RRID: AB_312963
CD45 (clone: 30-F11; BV510)	Biolegend	Cat# 103138; RRID: AB_2563061
CD62L (clone: MEL-14; FITC)	Biolegend	Cat# 104406; RRID: AB_313093
TCRβ (clone: H57-597; APC-Cy7)	Biolegend	Cat# 109220; RRID: AB_893624
TCRγδ (clone: GL3; PerCP-Cy5.5)	Biolegend	Cat# 118117; RRID: AB_10612572
Foxp3 (clone: FJK-16s; PE)	eBioscience	Cat# 12-5773-82; RRID: AB_465936
Rorγt (clone: Q31-378; BV421)	BD Bioscience	Cat# 562894; RRID: AB_2687545
IL-17A (clone: eBio17B7; PE)	eBioscience	Cat# 12-7177-81; RRID: AB_763582
IFNγ (clone: XMG1.2; FITC)	eBioscience	Cat# 11-7311-82; RRID: AB_465412
CD16/32 (clone: 2.4G2)	BD Bioscience	Cat# 553142; RRID: AB_394657
CD3ε (clone: 145-2C11)	Biolegend	Cat# 100359; RRID: AB_2616673
CD28 (clone: 37.51)	Biolegend	Cat# 102116; RRID: AB_11147170
Phospho-S6 ribosomal protein (Ser235/236) (clone: D57.2.2E; Alexa647)	Cell Signaling	Cat# 4851; RRID: AB_10695457
Chemicals, peptides, and recombinant proteins		
Tamoxifen	Sigma-Aldrich	Cat# T5648
Corn oil	Wako	Cat# 032-17016
Phorbol 12-myristate 13-acetate (PMA)	Sigma-Aldrich	Cat# P8139
Ionomycin	Sigma-Aldrich	Cat# I9657
Rapamycin	Sigma-Aldrich	Cat# R0395
Torin-1	Selleckchem	Cat# S2827
2-DG	Sigma-Aldrich	Cat# D8375
Fixable Viability Dye eFluor 780	eBioscience	Cat# 65-0865-14
Dithiothreitol (DTT)	Thermo Fisher Scientific	Cat# P2325
EDTA	Nacalai Tesque	Cat# 06894-85
Collagenase	Wako	Cat# 032-22364
DNase I	Sigma-Aldrich	Cat# DN25
Percoll	GE Healthcare	Cat# 1789101
Ammonium chloride	Nacalai Tesque	Cat# 02424-55
4% Paraformaldehyde Phosphate Buffer Solution	Wako	Cat# 163-20145
8% Glutaraldehyde	Wako	Cat# 533-08681
Agarose LM	Nacalai Tesque	Cat# 01161-54
Bovine serum albumin (BSA)	Nacalai Tesque	Cat# 01863-48
Triton-X100	Polysciences	Cat# 04605
DAPI	Dojindo	Cat# D523
Mouse Naïve $CD4^+$ T cell isolation kit	Miltenyi Biotech	Cat# 130-104-453
TGF-β	R&D systems	Cat# 7666-MB-005
Retinoic acid (RA)	Tokyo Chemical Industry	Cat# 0064-1G

(*Continued on next page*)

Continued

REAGENT or RESOURCE	SOURCE	IDENTIFIER
IFN-γ	Peprotech	Cat# 315-05
Fetal bovine serum (FBS)	Thermo Fisher Scientific	Cat# 10270-106
HBSS	Nacalai Tesque	Cat# 17460-15
RPMI1640	Nacalai Tesque	Cat# 30264-85
DPBS	Nacalai Tesque	Cat# 14249-24
Penicillin/streptmycin	Nacalai Tesque	Cat# 09367-34
Sodium pyruvate	Thermo Fisher Scientific	Cat# 11360070
MEM/NEAA	Thermo Fisher Scientific	Cat# 11140050
HEPES	Thermo Fisher Scientific	Cat# 15630080
β-mercaptoethanol	Thermo Fisher Scientific	Cat# 21985023
XF media	Agilent Technologies	Cat# 102353-100
TRIzol	Invitrogen	Cat# 15596018
Critical commercial assays		
iScript cDNA Synthesis Kit	BioRad	Cat# 170-8891
SYBR Green FAST qPCR Master Mix kit	Kapa Biosystems	Cat# KK4602
HypoxyprobeTM-1 Plus Kit	Hypoxyprobe I	Cat# HP2-100KIT
XF Cell Mito Stress Test Kit	Agilent Technologies	Cat# 103015-100
MitoTracker Green	Invitrogen	Cat# M7512
MitoTracker CMXROS	Invitrogen	Cat# M7152
TMRE-Mitochondrial Membrane Potential Assay Kit	Abcam	Cat# ab113852
Foxp3/transcription factor staining buffer set	eBioscience	Cat# 00-5523-00
2-NBDG Glucose Uptake Assay Kit	Biovision	Cat# K682-50
Anaeropack	Mitsubishi Gas Company	Cat# A-26
GoldiStop Protein Transport Inhibitor	BD Bioscience	Cat# 554724; RRID: AB_2869012
Experimental models: Organisms/strains		
Mouse: C57BL/6J	The Jackson Laboratory	JAX:000664
Mouse: *Cd4*^{cre}	The Jackson Laboratory	JAX:022071
Mouse: *Cd4*^{creERT2}	The Jackson Laboratory	JAX:022356
Mouse: *Hif1α*$^{fl/fl}$	Ryan et al., 2000	N.A.
Mouse: *Hif2α*$^{fl/fl}$	Gruber et al., 2007	N.A.
Mouse: *Vhl*$^{fl/fl}$	Haase et al., 2001	N.A.
Mouse: *Rptor*$^{fl/fl}$	Hoshii et al., 2014	N.A.
Mouse: *Rictor*$^{fl/fl}$	Magee et al., 2012	N.A.
Oligonucleotides		
QPCR primers	Hokkaido System Science	Table S1
Software and algorithms		
GraphPad Prism 8	GraphPad Software	https://www.graphpad.com/
FlowJo Vx software	TreeStar	https://www.flowjo.com/
ImageJ	ImageJ	https://imagej.net/Welcome
Imaris 8.4	Bitplane	https://imaris.oxinst.com

RESOURCE AVAILABILITY

Lead contact

Further information and requests for the resources and reagents should be directed and will be fulfilled by the lead contact, Tomohisa Sujino (tsujino1224@keio.jp).

Materials availability

All the mouse lines used in this study are available upon request.

This study did not generate new unique reagents.

Data and code availability

All the detailed data in this paper are available upon request.

This paper does not report original code.

Any additional information required to reanalyze the data reported in this paper is available from the lead contact upon request.

EXPERIMENTAL MODEL AND SUBJECT DETAILS

Mice

Mice used in this study were of a C57BL/6 background. *Cd4*^{cre}, *Cd4*^{creERT2}, *Rptor*$^{fl/fl}$, and *Rictor*$^{fl/fl}$, *Hif1α*$^{fl/fl}$, *Hif2α*$^{fl/fl}$, and *Vhl*$^{fl/fl}$ mice were previously described (Gruber et al., 2007; Haase et al., 2001; Hoshii et al., 2014; Magee et al., 2012; Ryan et al., 2000) and were maintained under specific pathogen-free (SPF) conditions in the Animal Care Facility of Keio University School of Medicine. Germ-free (GF) mice (C57BL/6 background strain) were purchased from Sankyo Lab Service Corporation and were kept in the GF Facility of Keio University School of Medicine. Both female and male mice were used for this study and were aged between 6 and 12 weeks at the time of experiments. All experiments were approved by the Institutional Review Board for Animal Experiments of Keio University and were performed according to the institutional guidelines and home office regulations.

METHOD DETAILS

Preparation of intraepithelial lymphocytes and lamina propria mononuclear cells

Mice were euthanized by cervical dislocation, and the small intestines were collected. After removal of residual fat tissue and Peyer's patches, the small intestine tissue was opened longitudinally and washed with Ca^{2+}, Mg^{2+}-free Hank's balanced salt solution (HBSS) (Nacalai Tesque) to remove fecal content. After washing, the small intestine was further cut into small pieces and incubated with HBSS containing 1 mM dithiothreitol (Invitrogen) and 5 mM EDTA (Nacalai Tesque) for 30 min at 37°C to remove the epithelial layer. After removal of the epithelial layer, the mucosal pieces were washed with HBSS and digested by incubation with HBSS containing 1.5% fetal bovine serum (Thermo Fisher Scientific), 1 mg/mL collagenase (Wako), and 0.1 mg/mL DNase (Sigma-Aldrich) for 30 min at 37°C. The digested solution was centrifuged at 1,700 rpm for 5 min. The pellet was resuspended in 40% Percoll (GE healthcare) and overlaid on 75% Percoll. Percoll gradient separation was performed by centrifugation at 2,000 rpm for 20 min at 20°C. Cells at the interphase were collected as LPL. For intraepithelial lymphocytes, the supernatant containing the epithelial layers was collected and centrifuged at 1,700 rpm for 5 min. The pellet was resuspended in 40% Percoll and overlaid on 75% Percoll. Percoll gradient separation was performed by centrifugation at 2,000 rpm for 20 min at 20°C. Cells at the interphase were collected as IEL.

Preparation of spleen cell suspensions

Spleens were harvested from the mice after death and homogenized manually in HBSS. The lysates were filtered through a cell strainer. The passed cells were hemolyzed with 0.84% (vol/wt) ammonium chloride (Nacalai Tesque), washed with HBSS, and collected for analysis.

Flow cytometry

Nonspecific staining was inhibited by incubation with anti-CD16/32 (BD Bioscience) for 20 min. The surface antigens of isolated single-cell suspensions were stained with the following antibodies: CD4 (RM4-5), CD8α (53-6.7), CD8β (eBioH35-17.2), CD45 (30-F11), TCRβ (H57-597), TCRγδ (GL3). For intracellular Foxp3 (FJK-16s) and RORγt (Q31-378) staining, cells were permeabilized using fixation/permeabilization solution (eBioscience) before intracellular staining with antibodies. For IL-17A (eBio17B7) and IFNγ (XMG1.2) staining, cells were incubated in Roswell Park Memorial Institute (RPMI)-1640 medium containing 10% fetal bovine serum (FBS) and 1% penicillin/streptomycin (Nacalai Tesque) with 50 ng/mL PMA (Sigma-Aldrich),

500 ng/mL ionomycin (Sigma-Aldrich), and GoldiStop (BD Bioscience). Cells were stained with antibodies against the indicated cell surface markers, and dead cells were stained with Fixable Viability Dye eFluor 780 (eBioscience). Cells were permeabilized using fixation/permeabilization solution before IL-17A and IFNγ staining. Spleen cell suspensions were stained with the following antibodies: CD45 (30-F11), TCRβ (H57-597), CD4 (RM4-5), CD8α (53-6.7), CD44 (IM7), and CD62L (MEL-14). For flow cytometry analysis, the FACS Canto system (BD Biosciences) was used. Data were analyzed by FlowJo Vx software (Tree Star). Cell sorting was performed using the BD FACS Aria II sorter (BD Biosciences). For measurement of mitochondrial mass and membrane potential, purified cells were washed with prewarmed RPMI-1640 medium (Nacalai Tesque) supplemented with 10% FBS (staining buffer). Approximately, 1.5×10^6 cells were resuspended in 1 mL of staining buffer containing MitoTracker Green (20 nM; M7514; Invitrogen) and MitoTracker CMXROS (20 nM; M7152; Invitrogen) and incubated in a CO_2 incubator at 37 °C for 30 min. Stained cells were washed with 1 mL of prewarmed staining buffer and used for FACS analysis or further staining with antibodies. For pS6 staining, $CD4_{IELs}$, $CD4_{LPLs}$ and spleen cells were stimulated for 30 min with soluble α-CD3 mAb (1 μg/mL), then fixed in phosphate-buffered saline (PBS)/2% paraformaldehyde for 20 min, permeabilized with 90% methanol for 30 min on ice, and then stained for CD4, CD45, TCRβ, TCRγδ, CD8α, CD8β and pS6 in PBS. All the antibodies were used at 1:200 dilution. Alternatively, TMRE (Abcam) was used to monitor mitochondrial membrane potential. Cells were incubated with 5 μM TMRE for 30 min at 37°C and washed in PBS.

Metabolic assays

OCR and ECAR were measured with an XF-24 analyzer (Seahorse Bioscience) according to the manufacturer's protocols. FACS-sorted 5×10^5 T cells were cultured in XF media (non-buffered Dulbecco's modified Eagle's medium containing 25 mM glucose, 2 mM L-glutamine, 1 mM sodium pyruvate, and 2% fetal bovine serum, Agilent Technologies). The assay was performed using XF Cell Mito Stress Test Kit (Agilent Technologies). Three baseline recordings were taken, and this was followed by the sequential injection of the ATP synthase inhibitor oligomycin (2.5 μM), the mitochondrial uncoupler carbonyl cyanide-4-(trifluoromethoxy)phenyl-hydrazone (FCCP; 0.5 μM), and the respiratory chain inhibitors antimycin A (1 μM) and rotenone (1 μM).

Quantitative real-time polymerase chain reaction

RNA was isolated using TRIzol (Invitrogen) according to the manufacturer's instructions. Complementary DNA was synthesized from the extracted RNA using the iScript cDNA Synthesis Kit (Bio-Rad). The obtained complementary DNA was amplified by quantitative real-time polymerase chain reaction (PCR) using primer sets and the SYBR Green FAST qPCR Master Mix kit (Kapa Biosystems). The house-keeping gene *Rpl32* was used for normalization of samples. Primer sequences used were listed in Table S1.

Transmission electron microscopy

Freshly sorted naïve $CD4^+$ T cells, SP_{IELs} and DP_{IELs} were immediately fixed with an equal amount of 4% glutaraldehyde and 4% paraformaldehyde in 0.1 M phosphate buffer pH 7.4 at 4°C overnight. Fixed samples were dehydrated and transferred to a fresh 100% resin to polymerize at 60°C for 48 h. The polymerized samples were ultra-thin sectioned at 70 nm with an ultramicrotome (Ultracut UCT, Leica) and observed by a transmission electron microscope (JEM-1400Plus, JEOL Ltd.).

In vivo tamoxifen treatment

Mice were gavaged for two consecutive days at the beginning of the week with 5 mg of tamoxifen (Sigma-Aldrich) dissolved in corn oil (Wako) at 50 mg/ml. After 5 weeks from first administration, mice were used for experiments.

In vivo treatment of rapamycin and 2DG

Mice were injected intraperitoneally with vehicle, rapamycin (8 mg/kg, Sigma-Aldrich) or 2DG (500 mg/kg, Sigma-Aldrich) daily for 5 weeks. Rapamycin and 2DG were first reconstituted in DMSO and then diluted with PBS.

Hypoxyprobe-1 staining

Mice were administrated pimonidazole (Hypoxyprobe, Burlington, MA) by intraperitoneal injection 30 min prior to sacrifice. Dissected pieces of mouse small intestine were washed in PBS and then fixed in 4% PFA

for overnight, 4°C. Tissue was embedded in 4% low melting temperature agarose (Nacalai Tesque) and cut into 200 μM sections using a Vibratome (Leica). Vibratome sections were washed in PBS and incubated with Blocking buffer (1% BSA, 1% mouse serum, 0.1% Triton-X100 in PBS) for 2 hours, room temperature. Sections were incubated with FITC conjugated α-pimonidazole monoclonal antibody (Hypoxyprobe, 1:100) for 1 hour, room temperature. PBS washed sections were counterstained with DAPI and mounted to analyze by confocal microscopy (Olympus FV3000)

In vitro $CD4^+CD8\alpha\alpha^+$ T cell differentiation

Naïve $CD4^+$ T cells were isolated by negative selection with mouse Naïve $CD4^+$ T cell isolation kit (Miltenyi). 1×10^5 cells were cultured for 4 days in 96-well plates precoated with 1 μg/ml of α-CD3ε (145-2C11; Biolegend) and 1 μg/ml of soluble α-CD28 (37.51; Biolegend) in RPMI 1640 media supplemented with 10% FBS, 1% penicillin/streptomycin, 1% pyruvate (11360070; Thermo Fisher Scientific), 1% MEM/NEAA (11140050; Thermo Fisher Scientific), 2.5% HEPES (15630080; Thermo Fisher Scientific), and 55 μM β-mercaptoethanol (21985023; Thermo Fisher Scientific) under $CD4^+CD8\alpha\alpha^+$ T cell conditions: RA (10 nM, 0064-1G, Tokyo Chemical Industry), TGFβ (2 ng/ml, 7666-MB-005, R&D systems), IFNγ (20 ng/ml, 315-05, Peprotech). For the treatment with inhibitors, Rapamycin (1 μM, Sigma-Aldrich), Torin-1 (1 μM, Selleckchem) and 2DG (1 mM, Sigma-Aldrich) were added into the cell culture. In some experiments, cells were placed inside a sealed air tight container which contains an anaeropack (Mitsubishi Gas Company, Tokyo, Japan). The anaeropack contains a gas-controlling reagent which absorbs oxygen and generates carbon dioxide resulting in a hypoxic atmosphere (8% O_2).

Analysis of glucose uptake

Glucose uptake was determined with a fluorescently labeled deoxyglucose analog (2-NBDG) using a commercially available kit (Biovision, Milpitas, CA, USA). Purified cells were washed twice with RPMI 1640 media supplemented with 0.5% FBS. Cells were resuspended in 400 μl of glucose-free medium supplemented with 150 μg/ml 2-NBDG and incubated at 37°C for 30 min. The cells were washed with assay buffer, and glucose uptake was quantified by FACS analysis.

QUANTIFICATION AND STATISTICAL ANALYSIS

Statistical analysis was performed using GraphPad Prism software. Data were analyzed by applying one-way analysis of variance or unpaired Student's t-test whenever necessary. A P value < 0.05 was considered significant.